



Seismic performance of fuel assemblies and impact force correlations with intensity-compatible sets of recorded ground motion time histories

Manuel Pellisetti ^{a,*}, Hannes Kessler ^a, Johannes Schmidl ^b, Andrii Nykyforchyn ^c, Sunay Staeuble-Akcay ^d

^a Framatome GmbH, Erlangen, Germany

^b NSSS Structural Engineer, Framatome GmbH, Erlangen, Germany

^c Director Earthquake Group, NPP Goesgen, Daeniken, Switzerland

^d Earthquake Engineer, NPP Goesgen, Daeniken, Switzerland



A B S T R A C T

In the present paper, the seismic performance of fuel assembly rows is analyzed for historical ground motion records of seismic events in Europe that are compatible with the seismic hazard background of Goesgen NPP, at the frequency of exceedance of $10^{-4}/\text{a}$. The benefit of the analysis is twofold. Firstly, it represents an alternative approach to standard fragility analysis, which is based on ground motions matching the UHS. Instead, the present analysis is based on recorded time histories which can be viewed as an actual earthquake scenario at the site.

Secondly, the analysis looks at ground motion intensity measures other than the peak ground acceleration, which are considered to be equally or even more relevant for actual damage. Ultimately, these results can lead to more realistic fragility estimates – and hence risk footprint in the PSA – of the FA.

1. Introduction

Row models of fuel assemblies are widely used to demonstrate adequate performance of fuel assemblies in light water reactors, as requested in the context of seismic design or beyond-design safety evaluations. In case of high seismic demands, fuel assemblies may experience impacts with neighboring fuel assemblies or with the core barrel. The seismic robustness of the fuel assemblies depends on spacer grid buckling. Resulting permanent spacer grid deformations at control-rod positions could slow down or hinder the control rod insertion. Therefore, permanent spacer grid deformations should not exceed specific design limits or should be excluded by limiting impact forces to remain below the buckling strength. The present paper focusses on impact forces. Robustness analyses based on the limitation of permanent spacer grid deformations are addressed in [Pellisetti et al. \(2015, 2017\)](#).

1.1. Scope

Seismic analysis of fuel assemblies are typically based on artificial time histories, matched to design response spectra or uniform hazard spectra (UHS) of the ground motion or even of floor response spectra.

The present paper aims at introducing additional realism in the

analysis of the seismic performance, by relying on recorded ground motion time histories. [Staeuble-Akcay et al. \(2018\)](#) used in their seismic structural analyses UHS-matched ground motion time histories and recorded time histories which are compatible with the macro-seismic intensity level VII to VIII and thus correspond to the target seismic hazard ENSI-2015 for the Goesgen site. Soil-structure interaction (SSI) analyses have been performed with these time histories to obtain in-structure responses. The responses that were calculated with the recorded time histories are used as input for dedicated dynamic models of the reactor pressure vessel (RPV) internals and, subsequently, of the fuel assemblies (FA), see [Fig. 1](#) below.

2. Ground motion

[Staeuble-Akcay et al. \(2018\)](#) selected from [EMSC \(2013\)](#) a set of 27 recorded time histories (see [Table 1](#)), compatible to the seismic hazard background at Goesgen:

- Frequency of exceedance of $10^{-4}/\text{a}$
- Magnitude $M_w = 5.6\text{--}6.7$
- Distance = 11–20 km
- Hypocenter depth $h = 6\text{--}11$ km
- Site Intensity VII–VIII

* Corresponding author.

E-mail addresses: manuel.pellisetti@framatome.com (M. Pellisetti), hannes.kessler@framatome.com (H. Kessler), johannes.schmidl@framatome.com (J. Schmidl), anykyforchyn@kkg.ch (A. Nykyforchyn), sstaeuble@kkg.ch (S. Staeuble-Akcay).

Nomenclature

BOL	Beginning-of-Life irradiation state
CA	Cluster Assembly
CAV	Cumulative Absolute Velocity, $CAV = \int_0^T a(t) dt$
ENSI	Eidgenössisches Nuklearsicherheitsinspektorat (Swiss Nuclear Regulatory Commission)
EOL	End-of-Life irradiation state
FA	Fuel Assembly
HTP	High Thermal Performance fuel assembly
I_A	Arias Intensity, $I_A = \frac{\pi}{2g} \int_0^T a(t)^2 dt$
IM	Intensity Measure
NPP	Nuclear Power Plant
PC	Principal Component
PGA	Peak Ground Acceleration
PGD	Peak Ground Displacement
PGV	Peak Ground Velocity
PSA	Probabilistic Safety Analysis
RPV	Reactor Pressure Vessel
SSI	Soil Structure Interaction
UHS	Uniform Hazard Spectrum
ν_0	average number of (upward) zero crossings per unit time
ν_1	average number of maxima per unit time

For each acceleration time history, the following set of intensity measures (IM) is evaluated with the Framatome Seismic Analysis Toolbox (SAT):

- PGA, PGV and PGD → peak ground acceleration, velocity and displacement.

- $I_A \rightarrow$ Arias intensity $I_A = \frac{\pi}{2g} \int_0^T a(t)^2 dt$, T being the duration of the signal, g the gravitational constant and a(t) the acceleration time history.
- T1, T2, T3 → times at which the cumulative I_A reaches 5%, 75% and 95% of the total I_A .
- CAV → cumulative absolute velocity $CAV = \int_0^T |a(t)| dt$.
- $\nu_0, \nu_1 \rightarrow$ number of upward zero-crossings per unit time and number of maxima per unit time.
- $E_{peak} \rightarrow$ average peak factor x_{max}/σ , where σ is the standard deviation of the time history.
- $E_{peak} \approx (2 \ln(N))^{1/2} + \gamma / (2 \ln(N))^{1/2}$ where $\gamma = 0.5772$ (Euler constant) and $N = 2 \nu_0 \cdot T$ is the number of half-cycles.
- Strong motion duration → T2-T1 (US definition) and T3-T1 (French definition)

3. Dynamic analysis of the fuel assembly response to seismic excitation

The loads on the fuel assemblies resulting from the ground motion are obtained via propagation through the following sequence of dynamic analysis models (see Fig. 1):

1. 3-D soil-structure-interaction analysis model of the Goesgen reactor building with SASSI, as described in Staeuble-Akcay et al. (2018).
2. 2-D horizontal model of the RPV internals with the non-linear dynamics code CESHOCK, as described in Hilpert et al. (2019).
3. 2-D horizontal models of the FA rows with the dedicated fuel accident analysis code of Framatome, KWUSTOSS, as described in Pellissetti et al. (2015).

Models #2 and #3 are two-dimensional models capturing horizontal

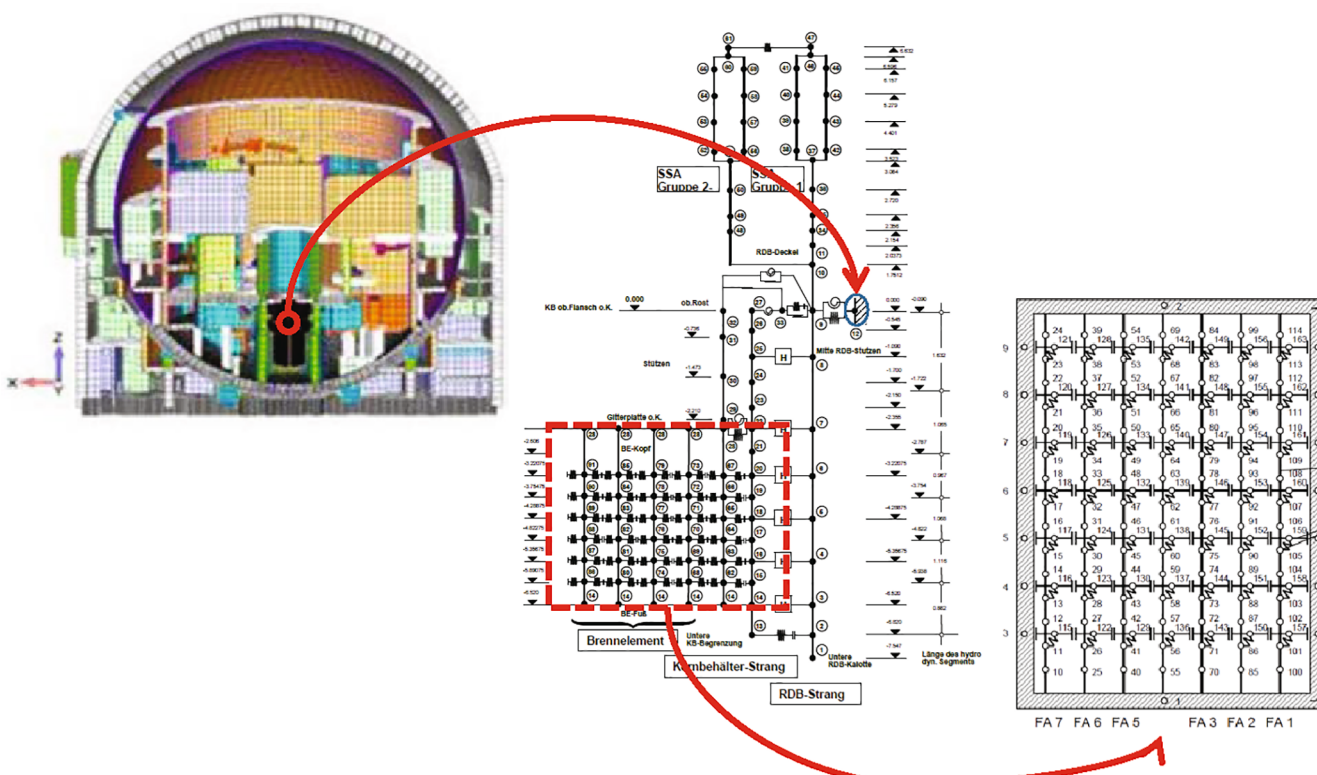


Fig. 1. Analysis cascade: reactor building (left); RPV including internals (middle); FA row (right).

Table 1

Ground motion records from EMSC (2013), used for the present analysis.

Record Number	Earthquake Name	Date	Station Name	M _w	Hypocenter Depth [km]	Distance Rjb [km]	PGA H1 [g]	PGA H2 [g]	Site Intensity (Sponheuer)	Intensity
367	Irpinia, Italy-02	23.11.1980	29 / Sturno	6.2	7	19	0.07	0.08	7.22	VII
566	Umbria	29.04.1984	122 / Nocera Umbra	5.7	9	19	0.22	0.17	6.78	VII
567	Umbria	29.04.1984	125 / Gubbio	5.7	9	13	0.04	0.05	7.29	VII
568	Umbria	29.04.1984	2735 / Umbertide	5.7	9	17	0.04	0.04	6.93	VII
569	Umbria	29.04.1984	2748 / Pietralunga	5.7	9	16	0.19	0.16	7.01	VII
576	Lazio Abruzzo	07.05.1984	49 / Cassino - Sant'Elia	5.9	11	18	0.15	0.11	7.43	VII
2151	Umbria Marche	26.09.1997	122 / Nocera Umbra	5.7	7	11	0.55	0.28	7.18	VII
2153	Umbria Marche	26.09.1997	126 / Borgo Cerreto - Torre	5.7	7	18	0.18	0.18	6.52	VII
2161	Umbria Marche	26.09.1997	119 / Castelnuovo (Assisi)	6.0	6	17	0.17	0.11	6.86	VII
2163	Umbria Marche	26.09.1997	121 / Assisi	6.0	6	14	0.19	0.17	7.12	VII
15240	Mt. Vatnafjoll	25.05.1987	209 / Minni-Nupur	6.0	8	19	0.03	0.02	7.09	VII
15903	Firuzabad	20.06.1994	3330 / Maymand	5.9	9	17	0.44	0.50	7.24	VII
15904	Firuzabad	20.06.1994	3331 / Kavar	5.9	9	16	0.04	0.03	7.32	VII
15905	Firuzabad	20.06.1994	1494 / Zarrat	5.9	9	15	0.31	0.26	7.40	VII
15906	Firuzabad	20.06.1994	3332 / Firoozabad	5.9	9	18	0.24	0.28	7.16	VII
17454	Edremit	09.11.2011	2508 / Van Merkez Bayindirlik Ve Iskan Mudurlugu	5.6	8	15	0.15	0.25	6.79	VII
103	Ionian	04.11.1973	2518 / Lefkada-O.T.E.	5.9	7	11	0.53	0.26	7.49	VIII
192	Volvi	20.06.1978	2657 / Thessaloniki-City Hotel	6.3	6	13	0.14	0.15	7.69	VIII
386	Alkion	25.02.1981	982 / Korinthos-O.T.E.	6.4	8	19	0.12	0.12	7.72	VIII
575	Lazio Abruzzo	07.05.1984	48 / Atina	5.9	11	11	0.10	0.12	8.09	VIII
844	Spitak	07.12.1988	2675 / Gukasian	6.7	6	20	0.19	0.18	7.76	VIII
9305	Avej	22.06.2002	2156 / Abgarm (Mokhaberat)	6.5	10	18	0.12	0.12	8.25	VIII
13220	Dahooeyeh-Zarand (Kerman)	22.02.2005	1518 / Chatrood	6.4	7	19	0.06	0.10	7.55	VIII
16834	L Aquila Mainshock	06.04.2009	3608 / Antrodoco	6.3	9	19	0.03	0.02	7.69	VIII
16848	L Aquila Mainshock	06.04.2009	3647 / Celano	6.3	9	20	0.09	0.08	7.62	VIII
16855	L Aquila Mainshock	06.04.2009	3664 / Fiamignano	6.3	9	17	0.03	0.02	7.84	VIII
16859	L Aquila Mainshock	06.04.2009	3680 / Gran Sasso (Lab. Infn Galleria)	6.3	9	19	0.03	0.02	7.69	VIII
16865	L Aquila Mainshock	06.04.2009	3709 / Montereale	6.3	9	16	0.06	0.04	7.92	VIII

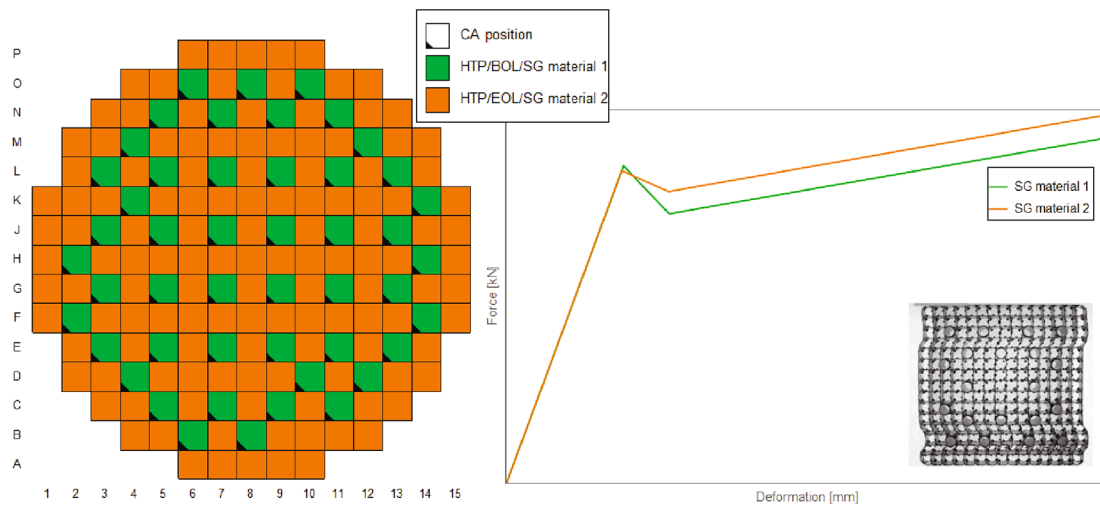


Fig. 2. Horizontal section through core (left); force–displacement curves of spacer grids (right).

translation and rotation in the associated vertical plane. Therefore two load cases are to be analyzed for each ground motion record:

- Load case “15”: 1 → global X axis in the building model (Fig. 1); 5 → rotation around Y
- Load case “24”: 2 → global Y, 4 → rotation around X

3.1. Core configuration

The analysed core configuration is shown in Fig. 2 below. It is a mixed core of HTP (High Thermal Performance) fuel assemblies (FA), designed and manufactured by Framatome ([Framatome Solutions Portfolio – PWR Fuel Assembly HTP](#)).

The mixed core accounts for FA in different irradiation states, with the following distribution:

- Control rod or cluster assembly (CA) positions (indicated by small black triangles in the left portion of Fig. 2): FA at beginning-of-life (BOL), with spacer grid material 1 (green squares)
- Non-control-rod-positions: FA at end-of-life (EOL), with spacer grid material 2 (orange squares)

The shapes of the idealized elastoplastic force versus total deflection curves of the spacer grids are indicated in the right portion of Fig. 2 below. Plastic deformations of the spacer grids occur in the nonlinear range after the buckling peak is exceeded. An exemplary plastically deformed spacer grid is also shown in Fig. 2.

3.2. Response quantity of interest

The response quantity of interest in the present analysis is the maximum impact force experienced by the spacer grids in model #3 during the seismic event. Distinction is made between fuel assemblies at control-rod position (cluster assembly, “CA”) and non control-rod positions (“non-CA”). For the success of control rod insertion, the fuel assemblies at control-rod position are relevant.

For each ground motion record, a total of six impact force data are evaluated, see Table 2.

Table 2
Quantities of interest.

	Maximum of all SG at CA positions	Maximum of all SG in the core
Load case 15	$F_{15,CA}$	$F_{15,tot}$
Load case 24	$F_{24,CA}$	$F_{24,tot}$
Load cases 15 and 24	F_{CA}	F_{tot}

4. Correlation analysis

4.1. Correlation between ground motion intensity measures

Fig. 3 shows the Pearson sample correlation coefficients between pairs of quantities ξ_i, η_i ,

$$r_{\xi\eta} = \frac{\sum \xi_i \eta_i - N \bar{\xi} \bar{\eta}}{\sqrt{(\sum \xi_i^2 - N \bar{\xi}^2)} \sqrt{(\sum \eta_i^2 - N \bar{\eta}^2)}} \quad (1)$$

where $\bar{\xi}$ and $\bar{\eta}$ are the sample means and N is the sample size. Intense red and blue colors indicate high positive and negative correlations, respectively.

Several observations can be made with the color map of the correlations:

There are two groups of intensity measures where the group members exhibit a strong positive correlation. These two groups are clearly visible in the correlation map, in the form of two large intensely colored red squares. The two groups include the following intensity measures:

- Group 1: peak ground acceleration, velocity and displacement (PGA, PGV, PGD); cumulative absolute velocity (CAV) and Arias intensity (I_A)
- Group 2: T_5 , T_{75} , T_{95} (time at which 5%, 75% and 95% of the I_A are reached); T_{US} (strong motion duration used in the US, T_{75} minus T_5), T_F (strong motion duration used in France, T_{95} minus T_5)

The remaining intensity measures are on one hand the average number of (upward) zero crossings (ν_0) and maxima (ν_1), per unit time,

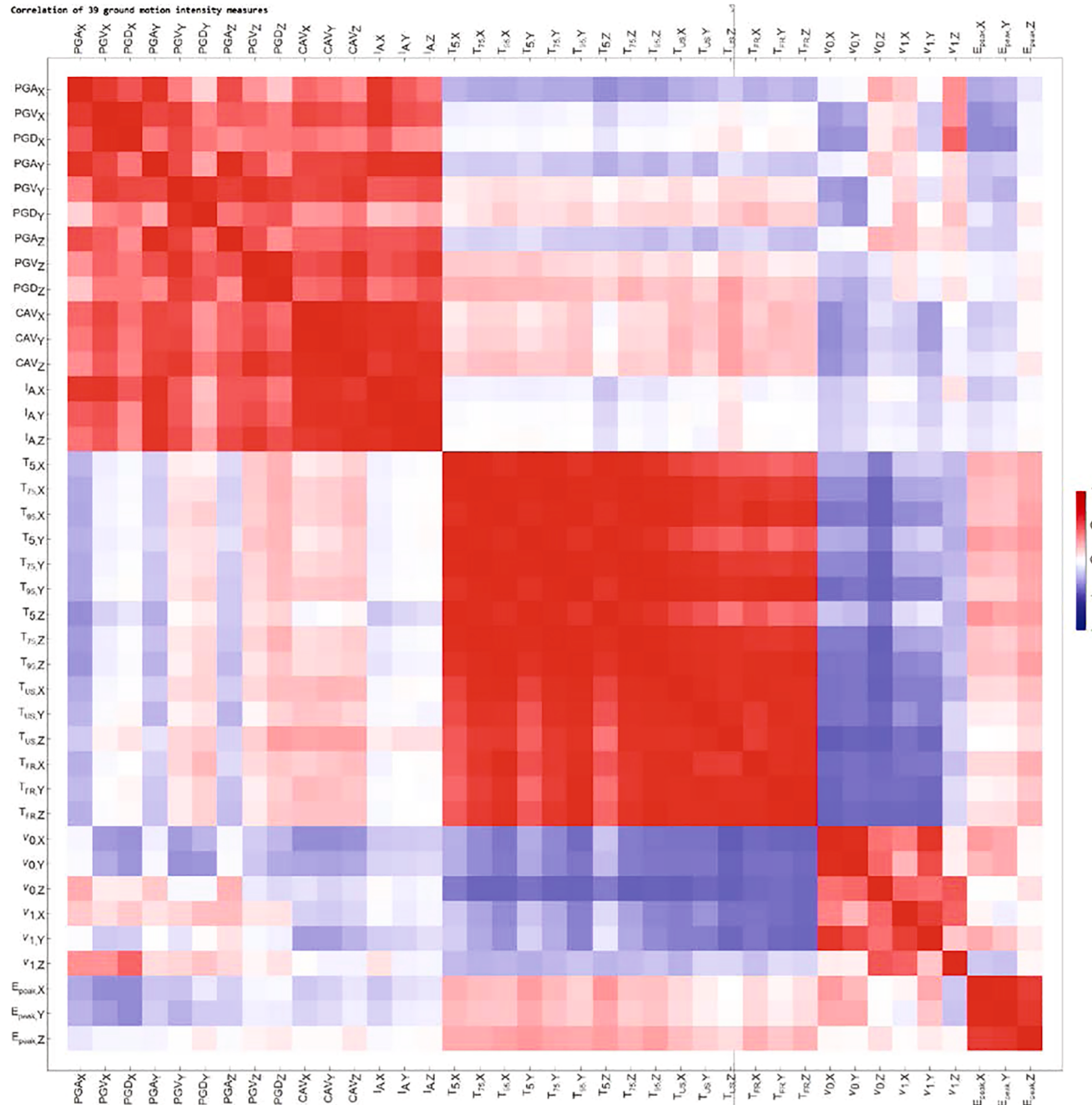


Fig. 3. Color map of the intensity measure correlation matrix.

respectively. These form a group of strong mutual correlation. However, they can be also viewed as members of an “extended Group 2”, because a clear negative correlation pattern with the members of Group 2 is visible. This pattern is represented by the blue rectangles to the right and below the “Group 2 square”.

Finally, the average peak factors E_{peak} (average of the peak factor representing the statistical distribution of the maximum of the random process, one for each direction) essentially form a group by themselves.

Within the groups of intensity measures, there is significant correlation between the different directions (e.g. PGA_X , PGA_Y and PGA_Z). The cross-direction correlation is somewhat lower for the PGD.

[Fig. 4](#) to [Fig. 6](#) examine the correlations in the three intensity measure groups more closely (including also the correlations between intensity measures and impact forces to be discussed below).

4.2. Correlation between individual ground motion intensity measures and impact forces

[Fig. 4](#) to [Fig. 6](#) can be further inspected for the correlation between

the intensity measures and the effects of the ground motion on the fuel assemblies, more specifically on the maximum impact forces (recall [Table 2](#)). The corresponding columns of the correlation matrix are the six rightmost columns in these Figures.

The correlation plot in [Fig. 4](#) clearly indicates a strong positive correlation between the peak ground accelerations, velocities and displacement and the maximum impact forces. The two intensity measures with the strongest correlation of around 90% to the maximum impact forces are the PGV (load case 15) and the Arias Intensity (load case 24).

In contrast, there is very little correlation between the Group 2 and 3 intensity measures (durations and peak factors) and the impact forces in [Fig. 5](#) and [Fig. 6](#), respectively.

Linear regression can be applied in a preliminary approach to analyze the dependence between impact forces and one of the intensity measures with a good correlation: [Fig. 7](#) displays for example the maximum impact force $F_{15,\text{tot}}$ versus the intensity measure PGV_X . Linear regression was applied in log-space, as described by [Zentner et al. \(2017\)](#),

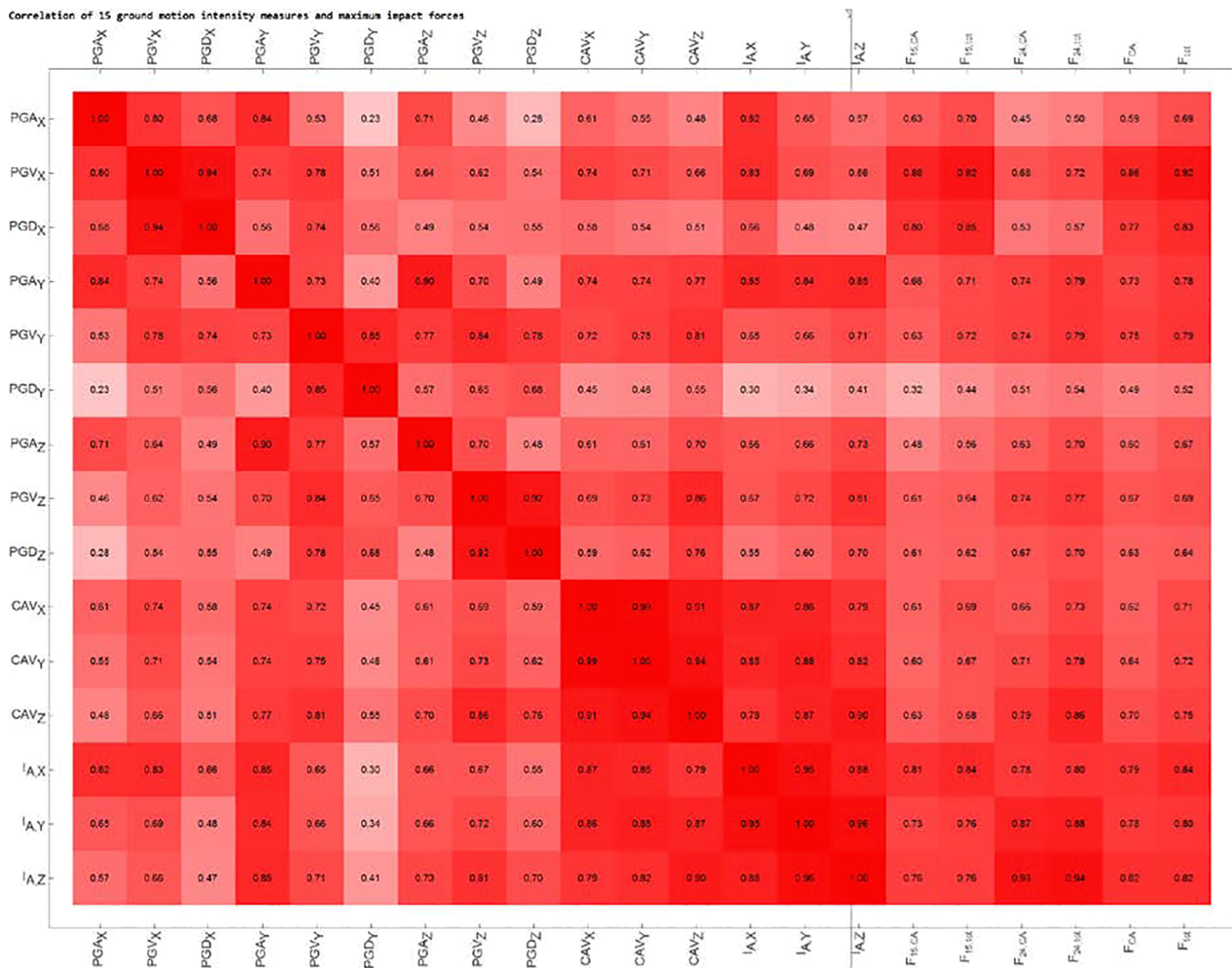


[Fig. 4](#). Correlation plot for group 1 intensity measures and impact forces.

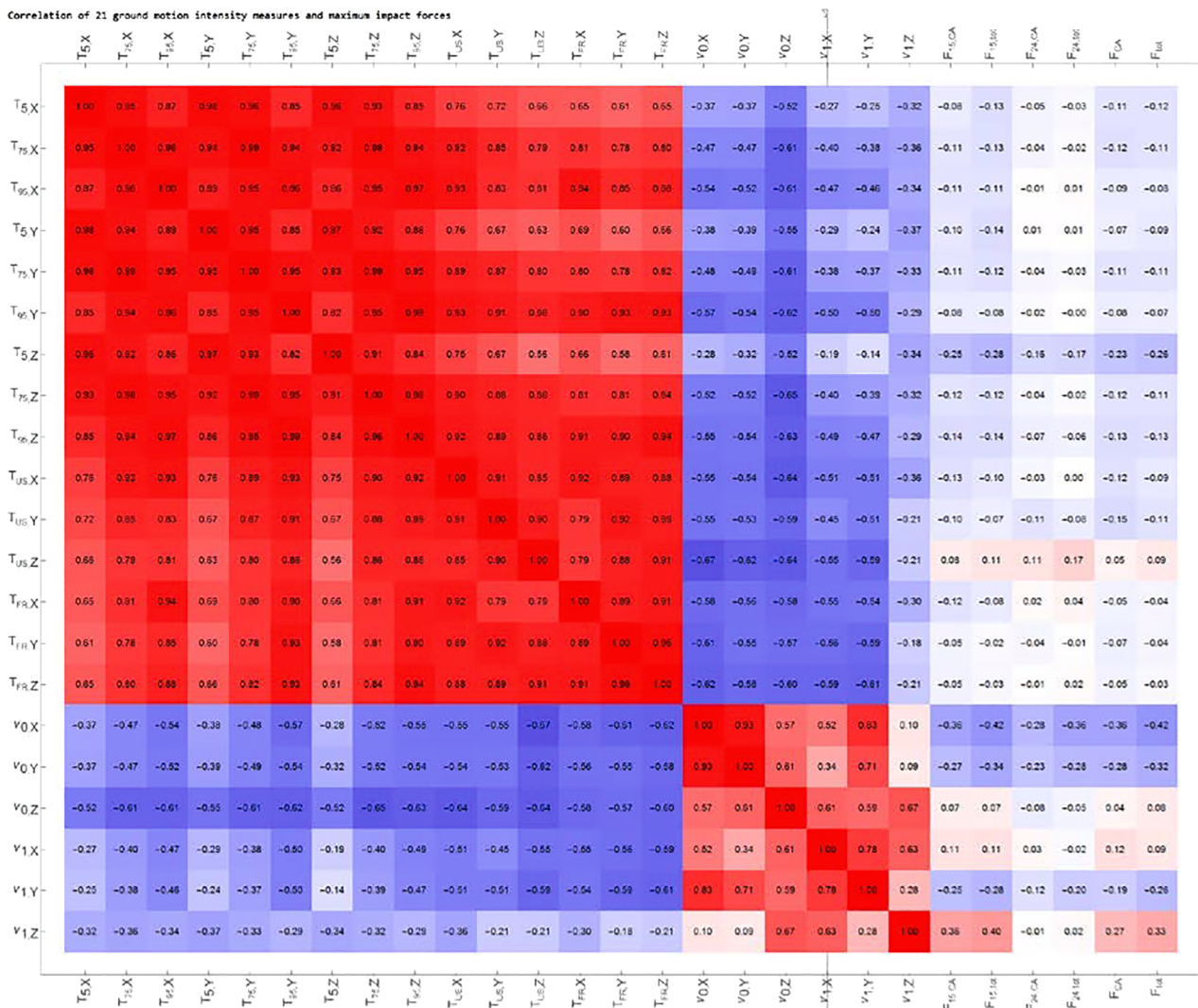


Fig. 5. Correlation plot for group 2 intensity measures and impact forces.

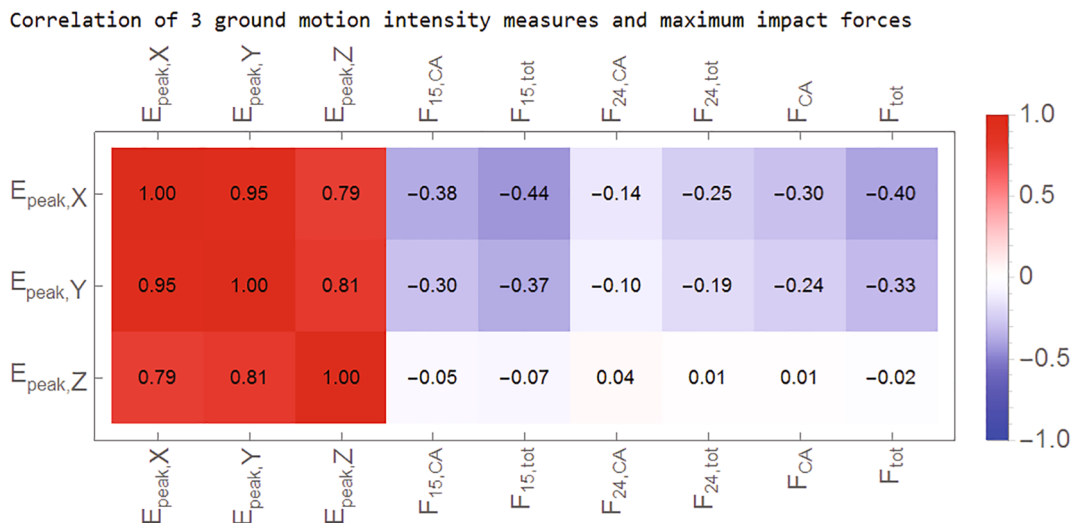


Fig. 6. Correlation plot for group 3 intensity measures and impact forces.

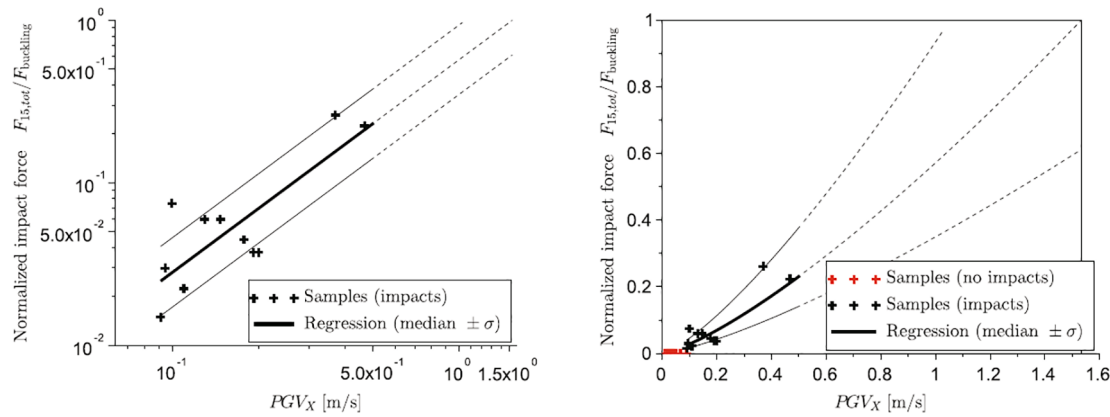


Fig. 7. Maximum impact force $F_{15,\text{tot}}$ (normalized with respect to buckling resistance) vs. PGV_X, logarithmic axes (left) and linear axes (right).

Eigenvector components with magnitudes > 0.15

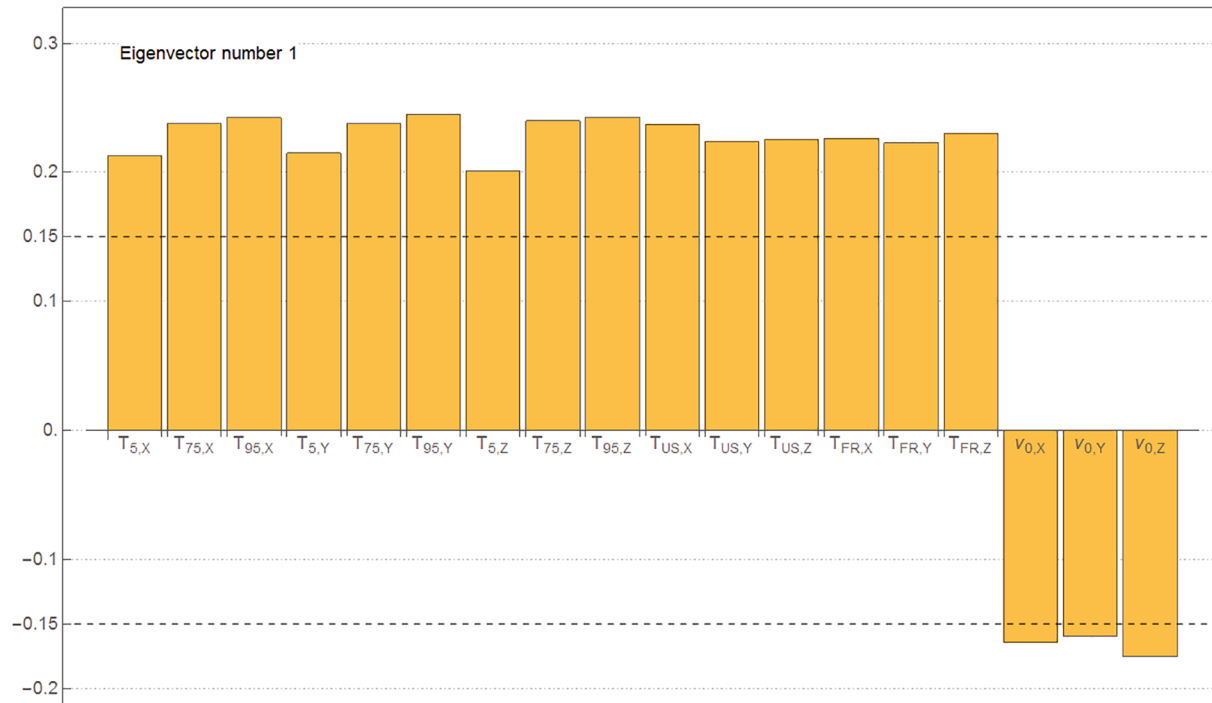


Fig. 8. Main intensity measure contributions to the 1st principal direction.

$$\ln Y = \ln b + c \ln \alpha + \sigma \varepsilon \quad (2)$$

In this case, Y represents the maximum impact force of a given time history, α represents the used intensity measure. The parameters b and c define the regression line, σ defines the standard deviation and ε is a standard normal random variable.

There are several ground motion records for which no impacts occur at all. These samples are plotted in red color in Fig. 7. Obviously these data cannot be used in determining the regression parameters, which are hence exclusively based on the data plotted in black.

The upper limit of the range of the vertical axis is given by the buckling strength. The results show that large margins exist, even for the two extreme events (records 15903 and 103).

It is important to keep in mind that the variability represented by σ – and hence by the $\pm \sigma$ uncertainty band in the regression diagram – is entirely due to the ground motion variability. Indeed, the 27 ground motion records are propagated through the same model. No simultaneous sampling of model parameters, such as stiffness or damping of ground, building or components, is performed. Using the fragility ter-

minology, the epistemic uncertainties associated with the analysis models are not included in the data shown in Fig. 7.

4.3. Principal component correlation analysis

The correlation between intensity measures and impact forces can be made more robust by a Karhunen-Loeve decomposition, which is the transformation of the vector of intensity measures to principal components of the intensity measure correlation matrix, Jolliffe (2004).

First, all intensity measures of all ground motion records are standardized by subtracting the means (of all ground motion records for a given intensity measure) and dividing by the standard deviations.

Second, the covariance matrix of the standardized intensity measures is formed (which is equal to the correlation matrix of the original non-standardized data).

Third, the eigenvalues and eigenvectors of the correlation matrix are calculated. The eigenvectors corresponding to different eigenvalues are mutually perpendicular. Eigenvectors of equal eigenvalues can be made perpendicular by the Gram-Schmidt procedure. All eigenvectors can be

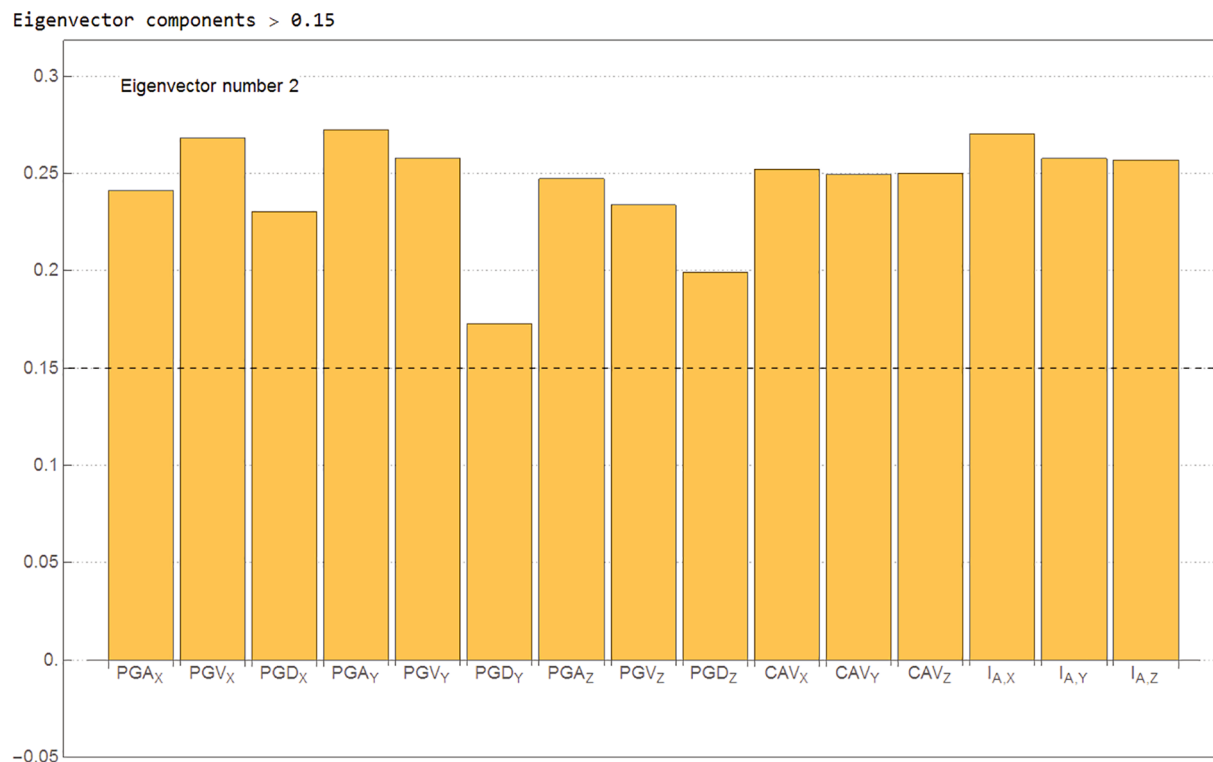


Fig. 9. Main intensity measure contributions to the 2nd principal direction.

Table 3

Correlations between IM principal components and impact forces Correlation between intensity measure principal components and positive impact forces.

	F _{15,C}	F _{15,tot}	F _{24,C}	F _{24,tot}	F _C	F _{tot}
PC ₁	-0.298	-0.028	0.102	-0.001	-0.194	-0.080
PC ₂	0.900	0.886	0.909	0.907	0.933	0.907
PC ₃	0.081	0.157	0.559	0.262	0.383	0.030

made of unit length. It is convenient to sort the eigenvectors from larger to smaller eigenvalues. There are 26 positive eigenvalues.¹ The principal components in the directions of eigenvectors with zero eigenvalues are identically zero; therefore these eigenvectors are omitted from further consideration.

Finally, the vector of the standardized intensity measures is transformed to principal components along the orthonormal eigenvectors of the intensity measure correlation matrix with non-zero (positive) eigenvalues. The resulting principal components in different directions are uncorrelated. Note that the total variance of all standardized intensity measures (given by the trace of the correlation matrix) is invariant with respect to the principal component transformation.

For the intensity measures alone, one could approximate the data by dropping principal components with sufficiently small eigenvalues (sufficiently small variance).² The first three principal components account already for almost 80% of the total variance and describe the intensity measure data already rather well. The first, second and third correlation scores are given by 40.7%, 28.8% and 9.7%, respectively.

¹ For 27 ground motion records there are at maximum 27 positive eigenvalues.

² The variability score of a principal component can be defined by the corresponding eigenvalue of the correlation matrix (equal to the variance of the principal component) divided by the sum of all eigenvalues (equal to the invariant total variance of all principal components / standardized intensity measures).

The first, second and third intensity measure principal components correspond roughly to the intensity measures in the extended group 2, group 1 and group 3 mentioned in the discussion of the correlation plots Fig. 3 to Fig. 6. This is illustrated in Fig. 8 and Fig. 9 which display the intensity measure components of the first and second eigenvector with magnitudes above a (somewhat arbitrary) threshold value 0.15. These leading intensity measure components are those of group 2 (Fig. 8, first eigenvector) and 1 (Fig. 9, second eigenvector). An increased threshold value of 0.34 would reveal the leading intensity measure components of group 3.

In order to analyze the correlation between intensity measures and impact forces, one has to take into account the correlation of the intensity measure principal components with the impact forces.

The second of the 26 nonzero principal components has the largest correlation to all force components. This is compatible with the observation that the group 1 intensity measure have the highest correlation with the impact forces according to Fig. 4 to Fig. 6.

Table 3 lists the correlations between the first three principal components and positive impact forces.³ The correlation values are used for a linear regression of the impact forces as function of the standardized intensity measures. Fig. 10 and Fig. 11 display the regression plots for the combined forces from both excitation directions (15 and 24) on control rod positions and in the whole core, respectively. The forces are normalized by the buckling strength of the spacer grids. The results show that large margins exist, even for the two extreme events (records 15,903 and 103). The vertical line crossing the intersection of the regression line with the horizontal axis indicates the impact threshold of the principal component as inferred from linear regression. The quality of the predicted impact threshold is rather good as only 2 ground motion records without impacts have a principal component above the impact

³ There are several ground motion records without impacts at all. These ground motion records are not taken into account for the correlation values in Table 3. Only ground motion records with impacts are used in linear regression of the forces.

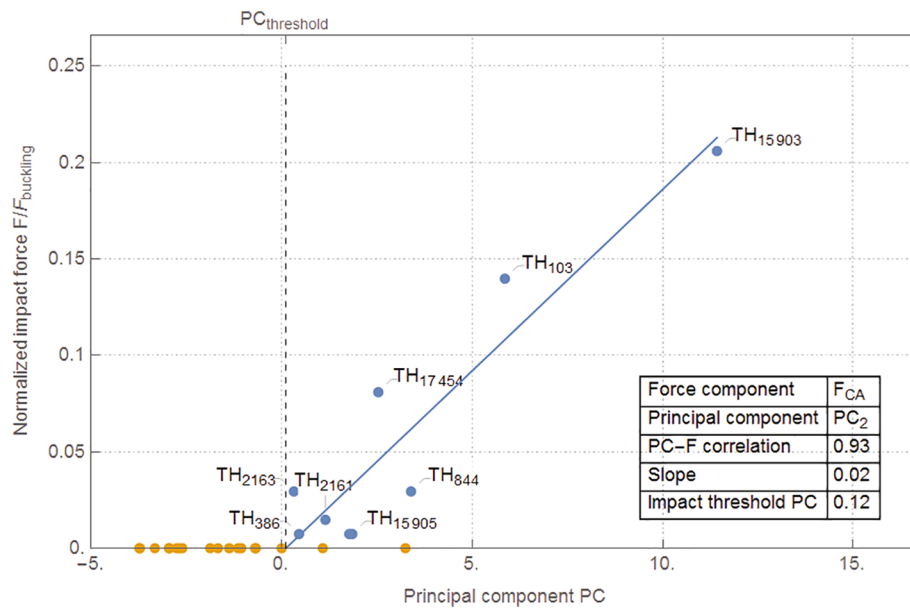


Fig. 10. Linear regression of impact forces on CA positions as function of the 2nd principal component.

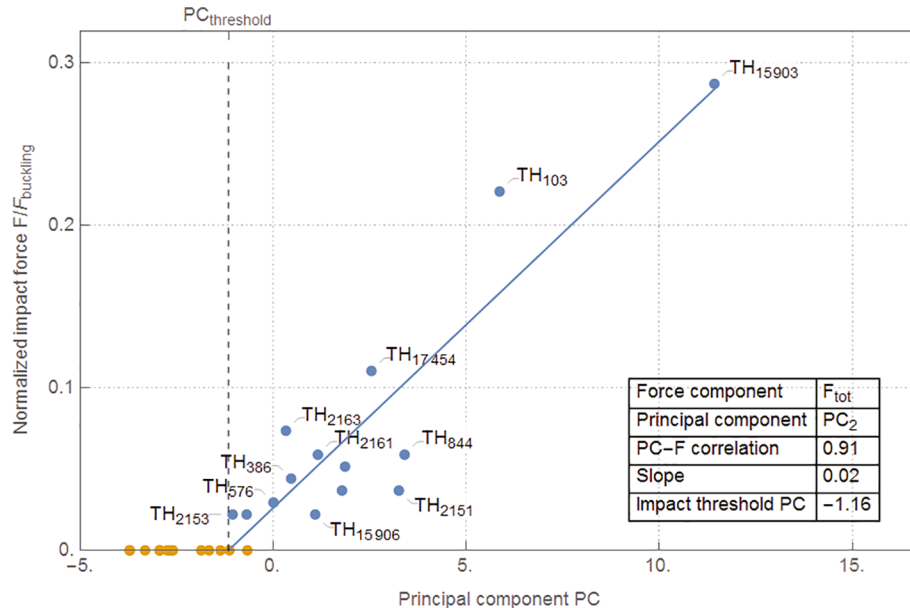


Fig. 11. Linear regression of impact forces in the core as function of the 2nd principal component.

threshold on the control rod positions in Fig. 10, and only 1 ground motion record without impacts in the whole core in Fig. 11.

5. Scaling of input excitation (fuel assembly row model)

For each of the 27 ground motion records, the last step of the analysis cascade in Fig. 1, that is the fuel assembly row model, is repeated with amplified input excitation. More specifically, the input excitation is amplified by a scaling factor of 2, 4 and 8, respectively. The purpose of this analysis is twofold. Firstly, it is possible to estimate for which scaling factor the maximum impact force reaches the buckling resistance of the spacer grids. Secondly, it provides insight as to whether the maximum impact force are somewhat proportional to the amplitude of the input excitation.

The results of this analysis are shown in Fig. 12. Two curves are shown for each of the 27 ground motion records, one for each horizontal

direction. In addition, Fig. 12 shows the same results for the two time histories that are representative of the 50% and the 84% fractiles of the floor response spectra based on the uniform hazard spectra (UHS) for $10^{-4}/\text{a}$. Several observations are suggested by the data:

1. For the shown range of scaling factors (1 through 8), the impact forces indeed scale more or less linearly with the amplitude of the input excitation. It is reiterated that in this analysis only the last step of the analysis cascade is repeated. Hence, the term input excitation refers to the motion of the upper and lower supports of the fuel assemblies in this case.
2. For all ground motion records, the maximum impact forces remain below the buckling resistance of the spacer grid if the fuel assembly input excitation is scaled by a factor of four or less. For almost all ground motion records, the maximum impact forces remain below the buckling resistance even if the fuel assembly input excitation is

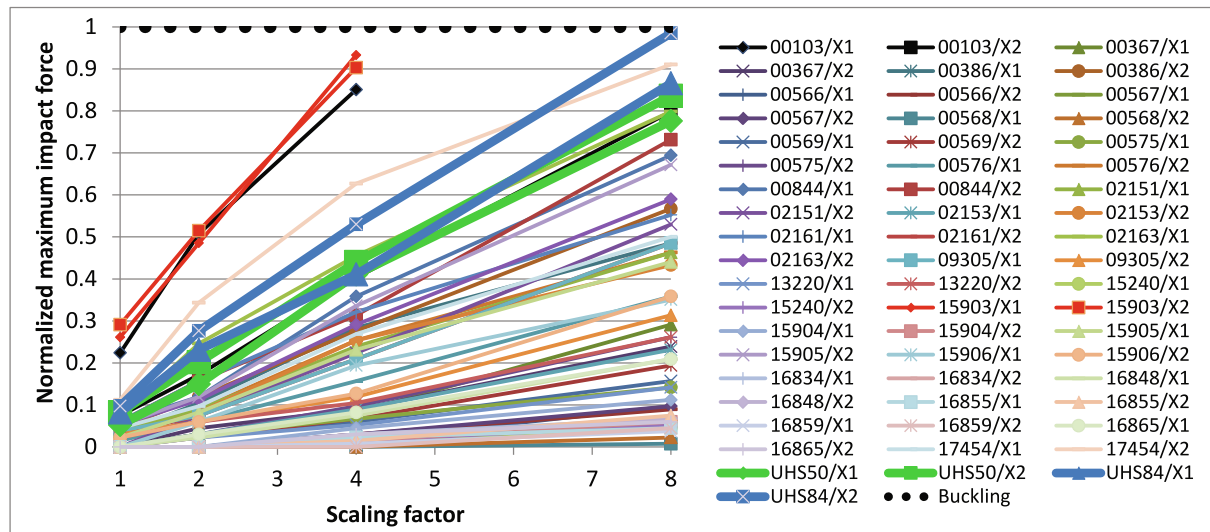


Fig. 12. Maximum impact force versus scaling factor applied to the input excitation of the fuel assembly row model.

scaled by a factor of eight. The exception are the two “outliers” in Fig. 4, that is records 15,903 and 103. For record 15903, the impact force exceeds the buckling resistance for a scaling factor below eight for both horizontal directions; for record 103 this is the case only for the horizontal direction Y (load case “24”). It is noted that for the outlier records 15,903 and 103, the permanent deformation resulting for a scaling factor of eight has been evaluated and found to be still in the admissible range.

3. The variability of the maximum impact forces is mainly driven by ground motion variability. This is suggested by the fact that the maximum impact forces corresponding to the 50% and the 84% fractiles of the UHS floor response spectra are relatively close to each other. The variability of the UHS is entirely due to the epistemic uncertainty of the soil-structure interaction model (damping and stiffness of soil and reactor building). This variability obviously translates to a smaller variability of the impact forces, compared to the ground motion variability, reflected by the curves corresponding to the 27 ground motion records.
4. The impact forces corresponding to the UHS excitations are enveloping the vast majority of the ground motion records, mostly by a large amount. Exceptions are the above mentioned outliers. This is in line with the comparison of floor response spectra performed by Stäuble-Akcay et.al. (2018).

6. Conclusions

In the present paper, the seismic performance of fuel assembly rows is analyzed for historical ground motion records of seismic events in Europe that are compatible with the seismic hazard background of Goesgen NPP, at the frequency of exceedance of $10^{-4}/a$.

The benefit of the analysis is twofold. Firstly, it represents an alternative approach to standard fragility analysis, which is based on ground motions matching the UHS. Instead, the present analysis is based on recorded time histories which can be viewed as an actual earthquake scenario at the site.

Secondly, the analysis looks at ground motion intensity measures other than the peak ground acceleration, which are considered to be equally or even more relevant for actual damage.

Ultimately, these results can lead to more realistic fragility estimates - and hence risk footprint in the PSA - of the FA.

The resulting maximum impact forces between fuel assembly spacer grids show that there are large margins with respect to the buckling resistance of the spacer grids. It is noted that the buckling resistance is a

conservative criterion, since limited permanent deformation of spacer grids is acceptable in the safety demonstration, as long as the rod insertion is still guaranteed.

Standard and principal component correlation analysis of the ground motion intensity measures and the impact forces show that there are two groups of strongly correlated intensity measures: one including the peak ground accelerations, velocities, displacements, the CAV and the Arias intensities; the other one including the parameters relevant for the duration. A particularly good correlation exists between impact forces and the individual intensity measures PGV and Arias intensity.

The impact forces strongly correlate with the first group (which contains the PGV and the Arias intensity). This is reflected by linear regression of the impact forces as function of the principal component of the intensity measures with the best correlation to the impact forces.

An important aspect of the principal component analysis is that it automatically groups highly correlated intensity measures by means of the eigenvectors. Thus, it is the analytical quantitative representation of the “families” of intensity measures that are emerging in a qualitative form from the correlation plots.

Amplification of the input excitation of the fuel assembly row model by scaling factors 2, 4 and 8 is performed. The maximum impact forces scale more or less linearly with the amplification factor.

The application of the scaling factors confirms the large margins: For all considered ground motion records, the maximum impact forces remain below the buckling resistance of the spacer grids even if the input excitation is scaled by a factor of 4. Furthermore, the allowable deformation is not exceeded even if the input excitation is scaled by a factor of 8.

The results also show that the impact forces corresponding to UHS are significantly larger than those resulting from most of the selected ground motion records.

Finally, it is remarked that the variability of the maximum impact forces is mainly driven by ground motion variability. In comparison, the effect of the epistemic uncertainty associated with the soil-structure interaction model is marginal.

Declaration of Competing Interest

The authors declare that they have no known competing financial interests or personal relationships that could have appeared to influence the work reported in this paper.

Acknowledgements

The first author acknowledges the support by the European Union's H2020-Euratom Program under grant agreement N° 755439 (NARSIS). The authors would like to thank Victor Hatman (Framatome Inc.) for his technical review comments.

References

EMSC, European-Mediterranean Seismological Centre, 2013, "RESORCE Reference Database for Seismic Ground-Motion in Europe", EMSC France.
 Framatome Solutions Portfolio – PWR Fuel Assembly HTP: www.framatome.com/solutions-portfolio/pages/product.aspx?l0=0&id=A0529.

- Hilpert, R., et al., 2019. "Nonlinear Finite Element Analysis of Seismic Loads on RPV Internals" SMiRT-25, Charlotte, NC, USA, August 4-9, 2019.
- Jolliffe, I.T., Principal Component Analysis, 2nd ed., New York: Springer, 2004.
- Pellissetti, M., Nykyforchyn, A., Rangelow, P., Schramm, K., Keßler, H., Klügel, J.-U., Klapp, U., 2015. "Seismic robustness of reactor trip via control rod insertion at increased seismic hazard estimates" SMiRT-23, Manchester, UK, August 10-14, 2015.
- Pellissetti, M., Keßler, H., Laudarin, F., Altieri, D., Nykyforchyn, A., Patelli, E., Klügel, J.-U., 2017. "Statistical analysis of impact forces and permanent deformations of fuel assembly spacer grids in the context of seismic fragility" SMiRT-25, Manchester, UK, August 20-25, 2017.
- Staeuble-Akcay, S., et al., 2018. "Seismic safety reassessment of NPP Goesgen after completion of site-specific probabilistic seismic hazard analysis" 16th European Conference on Earthquake Engineering, Thessaloniki, Greece, June 18-21, 2018.
- Zentner, M., Gündel, M., Bonfils, N., 2017. Fragility analysis methods: review of existing approaches and application. Nucl. Eng. Design 323 (2017), 245–258.